REVISTA INTERDISCIPLINAR DE PESQUISA EM ENGENHARIA

CILAMCE 2016
XXXVII IBERIAN LATIN AMERICAN CONGRESS ON COMPUTATIONAL METHODS IN ENGINEERING
BRASÍLIA - DF - BRAZIL

COMPUTATIONAL MODELING OF GRANULAR MATERIALS

Eduardo M. B. Campello

campello@usp.br

Department of Structural and Geotechnical Engineering

Polytechnic School, University of São Paulo

P.O. Box 61548, 05424-970, São Paulo, SP, Brazil

Abstract*. This work presents a computational model for the simulation of dry granular materials. The approach is based on the discrete element method (DEM), using phenomenological models to describe the various forces involved. A few numerical examples are provided to illustrate the potentialities of the proposed scheme. Consistent DEM models may be a useful tool for the study of granular materials and, in broader sense, many other particle systems.*

Keywords: *Granular materials; Discrete element method; Particles.*

1 INTRODUCTION

Granular materials and flows of granular matter can be found in a myriad of places and at various length scales, ranging from stone piles and rock sliding to fine powders and particulate flows, from mounds of sand and construction materials to compact aggregates of very high-added value in the pharmaceutical, chemical, food and microelectronics industries. The physics of such materials has evolved significantly over the past decades, especially with the aid of computational methods, but still there is a lot to pursue. The purpose of this work is to present, in a summarized and as simple a way as possible, a computational model for the simulation of dry granular materials. It is based on the so-called discrete element method (DEM), and in this sense can be viewed as one (among many possible) formulation of the DEM. For the sake of conciseness, only a brief description of the formulation is provided, with the interested reader being referred to Campello (2016) for details and a more rigorous representation. A few numerical examples are provided to illustrate the potentialities of the scheme. For an early history of the discrete element method, along with reviews on its application to the modeling of granular media, see Cundall and Strack (1979), Bicanic (2004), Pöschel and Schwager (2004), Zhu et al. (2008), O´Sullivan (2011) and Zohdi (2012), and references therein.

The paper is organized as follows. In Section 2 we describe our DEM formulation, including consistent representations for the several forces involved (in particular, a consistent stick-slip friction model is presented to properly capture inter-particle rolling motion). In Section 3 we present our time integration scheme for the solution of the system's dynamics, including an algorithmic overview. In Section 4 we show three examples of numerical simulations to illustrate the applicability of our scheme, and in Section 5 we close the paper with some final considerations. Throughout the text, plain italic letters ($a, b, \ldots, \alpha, \beta, \ldots, A, B, \ldots$) denote scalar quantities, boldface lowercase italic letters ($\boldsymbol{a}, \boldsymbol{b}, \ldots, \boldsymbol{\alpha}, \boldsymbol{\beta}, \ldots$) denote vectors and boldface italic capital letters ($\boldsymbol{A}, \boldsymbol{B}, \ldots$) denote second-order tensors in a three-dimensional Euclidean space. The (standard) inner product of two vectors is denoted by $\boldsymbol{u} \cdot \boldsymbol{v}$, and the norm of a vector by $\|\boldsymbol{u}\| = \sqrt{\boldsymbol{u} \cdot \boldsymbol{u}}$.

2 A FORMULATION OF THE DISCRETE ELEMENT METHOD

We follow the DEM approach proposed by the author Campello (2015) and Campello (2016) and treat collections of particles as discrete dynamical systems in which each particle interacts with the others and the surrounding media via a combination of various different forces. These are external field forces (from gravity, electric and/or magnetic exterior fields), drag forces, near-field forces (attractive and repulsive), adhesion forces, and contact and friction forces due to touching and collisions. Although these forces may (and, in the general case, do) act in the particles at the same time, the last two are certainly the dominant forces once we are concerned with granular materials in this work. Classical dynamics is adopted to describe the time evolution of the system, the equations of which are solved via a numerical (time-stepping) integration scheme. The particles are allowed to have both translational and rotational motions (in this sense, the model presented in this section may be seen as a generalization of the models presented by Campello and Zohdi (2014a, 2014b) and Campello (2015b), wherein rotations and spins were not considered). For the sake of simplicity, but without loss of generality, we consider here only spherical particles.

3.1 Equations of motion

Let the system be comprised of N_P particles, each one with mass m_i, radius r_i and electric charge q_i ($i = 1,...,N_P$). Let the center of a particle be designated by C_i, and the particle´s rotational inertia relative to it by $j_i = (2/5)m_i r_i^2$. Let $\{\mathrm{O}, \boldsymbol{e}_1, \boldsymbol{e}_2, \boldsymbol{e}_3\}$ be the global (fixed) reference system, with origin at point O, and let $\{\mathrm{C}_i, \boldsymbol{e}_{1,i}^{\ell}, \boldsymbol{e}_{2,i}^{\ell}, \boldsymbol{e}_{3,i}^{\ell}\}$ be the local (body-fixed) reference system of particle i, with origin at the particle´s center. We denote the position vector of a particle by $\boldsymbol{x}_i$, the velocity vector by $\boldsymbol{v}_i$ and the spin vector by $\boldsymbol{\omega}_i$, as depicted in Fig. 1. The rotation vector of a particle relative to the beginning of the motion, which furnishes the spatial orientation of the particle with respect to the initial configuration, is denoted by $\boldsymbol{\alpha}_i$, whereas the *incremental* rotation vector (i.e., rotation vector relative to two consecutive configurations) is denoted by $\boldsymbol{\alpha}_i^{\Delta}$. The rotational motion between two consecutive configurations is described by the incremental rotation tensor $\boldsymbol{Q}_i^{\Delta}$, which is a function of $\boldsymbol{\alpha}_i^{\Delta}$ and is given by the Euler-Rodrigues formula

$$\boldsymbol{Q}_i^{\Delta} = \boldsymbol{I} + \frac{4}{4 + \boldsymbol{\alpha}_i^{\Delta} \cdot \boldsymbol{\alpha}_i^{\Delta}} \left[\boldsymbol{A}_i^{\Delta} + \frac{1}{2} \boldsymbol{A}_i^{\Delta} \right], \tag{1}$$

wherein $\boldsymbol{A}_i^{\Delta} = \mathrm{Skew}(\boldsymbol{\alpha}_i^{\Delta})$ is the skew-symmetric tensor whose axial vector is $\boldsymbol{\alpha}_i^{\Delta}$. One should notice that the above expression referrers to a Rodrigues´ parameterization of the rotation tensor, instead of the usual one based on the Euler rotation vector. This implies that $\boldsymbol{\alpha}_i^{\Delta}$ is a Rodrigues rotation vector. We refer the reader to Campello (2015) for details. One should notice also that, though the particles are assumed to be spherical, the description of their rotations may be relevant to their motion, since inter-particle friction may induce rolling and thereby any material point P on the particle's surface (e.g., the contact point of a contacting pair) may move between two consecutive configurations – a motion that involves rotation and needs to be mapped if one is interested in properly capturing stick-slip phenomena. This issue will become clearer in forthcoming equations. In Fig. 1, vector $\boldsymbol{r}_i^{\mathrm{P}}$ is the vector that locates a material point P on the surface of the particle with respect to the particle´s center.

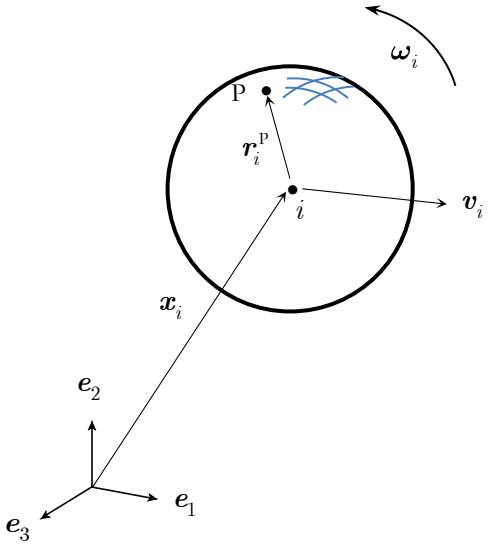

Fig. 1 Description of a single particle. Point P is on the particle's surface and may represent, e.g., the point of contact with another particle or object

Let us denote the total force vector acting on particle i by $\boldsymbol{f}_i^{tot}$ and the total moment

(with respect to the particle´s center) by $\boldsymbol{m}_i^{tot}$. According to the Euler´s laws, at every time instant t the following equations must hold for each particle:

$$\begin{aligned} m_i\ddot{\boldsymbol{x}}_i &= \boldsymbol{f}_i^{tot}, \\ j_i\dot{\boldsymbol{\omega}}_i &= \boldsymbol{m}_i^{tot}, \end{aligned} \tag{2}$$

where the superposed dot denotes differentiation with respect to time. The total force vector is made up of several force contributions as follows

$$\boldsymbol{f}_i^{tot} = \boldsymbol{f}_i^{ef} + \boldsymbol{f}_i^{drag} + \boldsymbol{f}_i^{nf} + \boldsymbol{f}_i^{adh} + \boldsymbol{f}_i^{con} + \boldsymbol{f}_i^{fric}, \tag{3}$$

in which $\boldsymbol{f}_i^{ef}$ are the forces due to external fields (gravity, electric and/or magnetic exterior fields), $\boldsymbol{f}_i^{drag}$ is the drag force vector (it stands for viscous effects induced by the surrounding medium on the motion of the particle), $\boldsymbol{f}_i^{nf}$ are the forces due to near-field interactions with other particles, $\boldsymbol{f}_i^{adh}$ are the forces due to adhesion to other particles and/or objects, $\boldsymbol{f}_i^{con}$ are the forces due to mechanical contacts (or collisions) with other particles and/or obstacles, and $\boldsymbol{f}_i^{fric}$ are the forces due to friction that arise from these contacts or collisions. The total moment vector, in turn, has contributions only from the friction forces, since all other forces are assumed to be central forces (i.e., they act with no eccentricity relatively to the center of the particle), such that

$$\boldsymbol{m}_i^{tot} = \boldsymbol{m}_i^{fric}. \tag{4}$$

Each one of the force and moment contributions above is (briefly) described in the subsections that follow. For more details on these forces, we refer the reader to Campello (2016).

3.2 External fields force

External fields are defined here by a gravity acceleration vector $\boldsymbol{g}$, an electric field vector $\boldsymbol{E}$ and a magnetic field vector $\boldsymbol{B}$, acting on the system. These fields are assumed here to be fully uncoupled and static, in the sense that they are not affected by the motion of the particles. The forces they induce on particle i are given by

$$\boldsymbol{f}_i^{ef} = m_i\boldsymbol{g} + q_i\boldsymbol{E} + q_i\boldsymbol{v}_i \times \boldsymbol{B}\,. \tag{5}$$

The sum of the two last terms in (5) is the so-called Lorentz force. We remark that the influence of auto-induced electromagnetic fields (i.e., those generated by the particles themselves) is considered negligible, since the particles are expected to experience translational velocities that are way below the speed of light.

3.3 Drag force

The drag force has origins in the friction and pressure that the surrounding medium exerts on a particle. It is given here by

$$\boldsymbol{f}_i^{drag} = -\frac{1}{2}\rho_F C_D A_i \|\boldsymbol{v}_i - \boldsymbol{v}_F\|(\boldsymbol{v}_i - \boldsymbol{v}_F)\,, \tag{6}$$

where ρ_F is the mass-density of the fluid, C_D is the drag coefficient, $A_i = \pi r_i^2$ is the "frontal" area of the particle with respect to the flow, and $\boldsymbol{v}_F$ is the (local) velocity of the fluid. The drag coefficient is assumed here to be a function of the Reynolds number of the flow, according to the model by Biringen and Chow (2011) as follows

$$\text{For } \ 0 < \mathrm{Re} \leq 1, \quad C_D = 24(\mathrm{Re})^{-1}; \tag{7}$$

$$\text{For } \ 1 < \mathrm{Re} \leq 400, \quad C_D = 24(\mathrm{Re})^{-0,646}; \tag{8}$$

$$\text{For } \ 400 < \mathrm{Re} \leq 3\times 10^5, \quad C_D = 0,5; \tag{9}$$

$$\text{For } \ 3\times 10^5 < \mathrm{Re} \leq 2\times 10^6, \quad C_D = 0,000366(\mathrm{Re})^{0,4275}; \tag{10}$$

$$\text{For } \ \mathrm{Re} > 2\times 10^6, \quad C_D = 0,18, \tag{11}$$

where Re is given by

$$\mathrm{Re} = \frac{2r_i\rho_F \|\boldsymbol{v}_i - \boldsymbol{v}_F\|}{\eta_F}, \tag{12}$$

with η_F as the viscosity of the fluid. The assumption of C_D being dependent on Re is valid for incompressible fluids, which is the case here (we assume that the relative velocity between the fluid and the particles is below the speed of sound in the fluid).

3.4 Near-field forces

The forces due to near-field (electromagnetic) interactions with other particles are given by

$$\boldsymbol{f}_i^{nf} = \sum_{j=1, j\neq i}^{N_P} \boldsymbol{f}_{ij}^{nf}, \tag{13}$$

where $\boldsymbol{f}_{ij}^{nf}$ is the near-field force that acts on particle i due to particle j. This force has the general expression

$$\boldsymbol{f}_{ij}^{nf} = \kappa_1 \left\|\boldsymbol{x}_i - \boldsymbol{x}_j\right\|^{-\lambda_1} \boldsymbol{n}_{ij} - \kappa_2 \left\|\boldsymbol{x}_i - \boldsymbol{x}_j\right\|^{-\lambda_2} \boldsymbol{n}_{ij}, \tag{14}$$

in which the κ´s and λ´s are scalar parameters dictating the intensity of the force for the pair $\{i, j\}$ and $\boldsymbol{n}_{ij}$ is the unit vector that points from the center of particle i to the center of particle j, i.e.,

$$\boldsymbol{n}_{ij} = \frac{\boldsymbol{x}_j - \boldsymbol{x}_i}{\left\|\boldsymbol{x}_j - \boldsymbol{x}_i\right\|}. \tag{15}$$

This vector will be referred to as the pair´s central direction from now on. In equation (14), scalars κ_1 and λ_1 are related to the attractive part of the force, whereas κ_2 and λ_2 to the repulsive part. This expression may be understood as derived from a generalized Mie´s potential (force potential for atomic and molecular interactions), of which the classical

Lennard-Jones potential (see Lennard-Jonnes (1924)) is a special case. It can be used to model e.g. van de Waals effects, electrostatic interactions, etc.

3.5 Adhesion forces

The forces due to adhesion to other particles and/or objects are given here by

$$\boldsymbol{f}_i^{adh} = \sum_{j=1}^{N_i^{adh}} \boldsymbol{f}_{ij}^{adh} \,, \tag{16}$$

where N_i^{adh} is the number of particles and/or objects that are adhered to particle i and $\boldsymbol{f}_{ij}^{adh}$ is the adhesion force on particle i due to particle or object j. This force has the general expression

$$\boldsymbol{f}_{ij}^{adh} = k^{adh}(\varepsilon_{ij})^{\beta}\boldsymbol{n}_{ij} \,, \quad \varepsilon_{ij} \geq \varepsilon_c \,, \tag{17}$$

where k^{adh} is a parameter related to the stiffness of the force, β is a material parameter and ε_{ij} is a measure of the local deformation of the pair $\{i,j\}$ at their point of adhesion, given here by

$$\varepsilon_{ij} = \frac{|\delta_{ij}|}{r_i + r_j}, \tag{18}$$

where δ_{ij} is the amount of overlap or penetration between the pair. This, it turn, is given by

$$\delta_{ij} = \|\boldsymbol{x}_i - \boldsymbol{x}_j\| - (r_i + r_j). \tag{19}$$

In expression (17), ε_c is a critical value of the deformation that dictates whether the adhesion force is turned on or off. It must be pre-specified.

3.6 Contact forces

The forces due to contacts or collisions with other particles and/or objects are described here with an overlap-based scheme (also usually called a soft-sphere model). Accordingly, they are a function of the amount of overlap between the pair in contact. We follow Hertz´s elastic contact theory (see e.g. Johnson (1985)) and adopt the following expression for $\boldsymbol{f}_i^{con}$:

$$\begin{aligned} \boldsymbol{f}_i^{con} &= \sum_{j=1}^{N_i^{con}} \boldsymbol{f}_{ij}^{con}, \quad \text{with} \\ \boldsymbol{f}_{ij}^{con} &= \frac{4}{3}\sqrt{r^*}E^*\delta_{ij}^{3/2}\boldsymbol{n}_{ij} + d^*\dot{\delta}_{ij}\boldsymbol{n}_{ij} \,, \end{aligned} \tag{20}$$

where N_i^{con} is the number of particles and/or objects that are in contact with particle i, $\boldsymbol{f}_{ij}^{con}$ is the contact force that acts on particle i due to particle or object j,

$$r^* = \frac{r_i r_j}{r_i + r_j} \quad \text{and} \quad E^* = \frac{E_i E_j}{E_j(1-\nu_i^2) + E_i(1-\nu_j^2)} \tag{21}$$

are the effective radius and the effective elasticity modulus of the contacting pair $\{i, j\}$ (in which E_i, E_j and ν_i, ν_j are the elasticity modulus and the Poisson coefficient of i and j, respectively), δ_{ij} and $\dot{\delta}_{ij}$ are the overlap and overlap velocity between the pair, and

$$d^* = 2\xi_n \sqrt{2E^* m^* \sqrt{r^*}} \left|\delta_{ij}\right|^{1/4} \tag{22}$$

is a damping constant that is introduced to allow for energy dissipation in the pair´s central direction. This constant is taken here following the ideas of Wellmann and Wriggers (2012), wherein ξ_n is the damping rate of the collision (which must be specified) and m^* is the effective mass of the contacting pair, i.e.,

$$m^* = \frac{m_i m_j}{m_i + m_j} \,. \tag{23}$$

The value of ξ_n may be related to an equivalent coefficient of restitution e (a simplified way is through $\xi_n = -\ln e \,/\, (\pi^2 + \ln^2 e)^{1/2}$, which is derived by assuming constant stiffness and constant damping throughout the collision, leading to a velocity-independent e – this is arguable but commonly adopted). We refer the interested reader to Pöschel and Schwager (2004) for several possibilities and a thorough discussion on the subject. Fig. 2 (top part) provides a schematic illustration of the contact/collision for a contacting pair.

3.7 Friction forces

The forces due to friction (which arise from the contacts/collisions) are given by

$$\boldsymbol{f}_i^{fric} = \sum_{j=1}^{N_i^{con}} \boldsymbol{f}_{ij}^{fric} \,, \tag{24}$$

where $\boldsymbol{f}_{ij}^{fric}$ is the friction force that acts on particle i due to particle j. This force is applied at the contact point P on the surface of particle i (see Fig. 2, bottom part), and is modeled here by assuming that sliding and rolling may occur between the contacting pair (whether it is pure sliding, sliding with rolling or pure rolling depends on the motion and properties of the pair). To describe such phenomena, we devise a scheme that is based on a tangential spring-dashpot system, placed at the contact point in the contact´s tangential direction. Consistent with stick-slip friction models, first we assume that sticking is to occur between the contact points of the contacting pair. The friction force that will cause such sticking is then applied gradually by the spring-dashpot system, being called a *trial* friction force, with the condition that the static friction limit is not violated. In case a violation is observed, sliding is to occur and thereby the friction force is the dynamic friction. The model reads as follows:

$$\boldsymbol{f}_{ij}^{fric,\mathrm{trial}} = -(k^{fric} \boldsymbol{\Delta x}_{ij}^{\mathrm{trial}} + d^{fric} \boldsymbol{v}_{ij}), \tag{25}$$

where k^{fric} is the stiffness of the spring, is the damping constant of the dashpot, $\boldsymbol{\Delta x}_{ij}^{\mathrm{trial}}$ is the trial elongation of the spring and $\boldsymbol{v}_{ij}$ is the elongation velocity. The trial elongation is given by

$$\boldsymbol{\Delta x}_{ij}^{\mathrm{trial}} = \boldsymbol{\Delta x}_{ij}^{\mathrm{accum}} + \delta \boldsymbol{x}_{ij}^{\mathrm{trial}} \,, \tag{26}$$

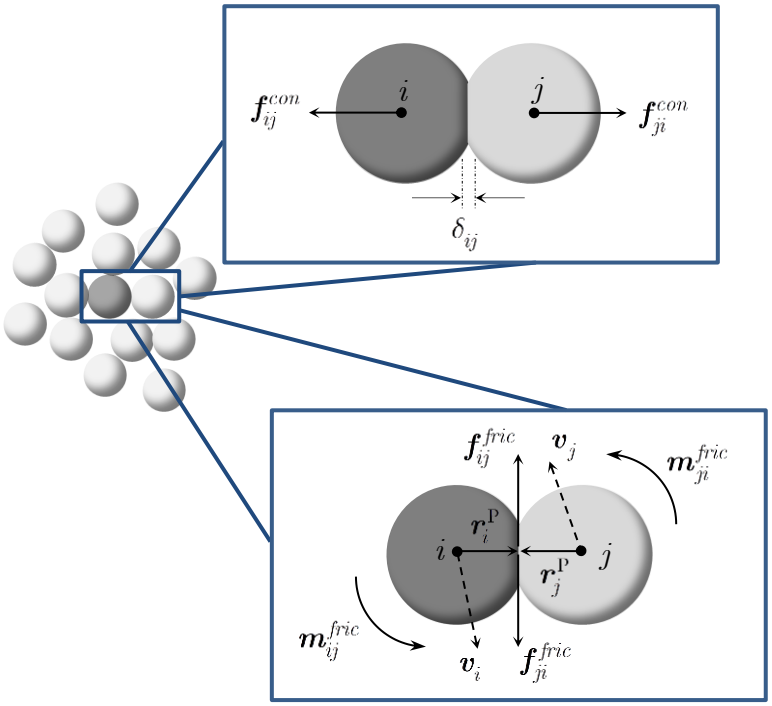

Fig. 2 Contact/collision between two particles

where $\Delta\boldsymbol{x}_{ij}^{\mathrm{accum}}$ is the accumulated elongation until then (i.e., elongation acquired in previous configurations, which must be stored) and $\delta\boldsymbol{x}_{ij}^{\mathrm{trial}}$ is the trial *incremental* elongation, i.e., is the increase in the elongation observed at the current configuration, whose expression will be shown shortly below. The elongation velocity is taken as the relative velocity of the contact points of i and j in the tangential direction, i.e.,

$$\boldsymbol{v}_{ij} = \boldsymbol{v}_{rel,t}^{\mathrm{P}} = \boldsymbol{v}_{rel}^{\mathrm{P}} - (\boldsymbol{v}_{rel}^{\mathrm{P}} \cdot \boldsymbol{n}_{ij})\boldsymbol{n}_{ij}\,, \tag{27}$$

where

$$\boldsymbol{v}_{rel}^{\mathrm{P}} = \boldsymbol{v}_i^{\mathrm{P}} - \boldsymbol{v}_j^{\mathrm{P}} \tag{28}$$

and, in turn,

$$\boldsymbol{v}_i^{\mathrm{P}} = \boldsymbol{v}_i + \boldsymbol{\omega}_i \times \boldsymbol{r}_i^{\mathrm{P}} \quad \text{and} \quad \boldsymbol{v}_j^{\mathrm{P}} = \boldsymbol{v}_j + \boldsymbol{\omega}_j \times \boldsymbol{r}_j^{\mathrm{P}}\,. \tag{29}$$

The direction of the trial friction force, denoted by $\boldsymbol{t}_{ij}^{\mathrm{trial}}$, is given by

$$\boldsymbol{t}_{ij}^{\mathrm{trial}} = \frac{\boldsymbol{f}_{ij}^{fric,\mathrm{trial}}}{\left\|\boldsymbol{f}_{ij}^{fric,\mathrm{trial}}\right\|}. \tag{30}$$

In order to verify whether the sticking assumption is valid or not, we define a sliding criterion function F, given by

$$F(\boldsymbol{f}_{ij}^{fric}) = \left\|\boldsymbol{f}_{ij}^{fric}\right\| - \mu_S \left\|\boldsymbol{f}_{ij}^{con}\right\|, \tag{31}$$

such that

$$\begin{cases} F(\boldsymbol{f}_{ij}^{fric,\mathrm{trial}}) \leq 0 \Rightarrow \text{the assumption is valid (sticking occurs)}; \\ F(\boldsymbol{f}_{ij}^{fric,\mathrm{trial}}) > 0 \Rightarrow \text{the assumption is not valid (sliding occurs)}. \end{cases} \tag{32}$$

In (31), μ_S is the static friction coefficient. If the assumption is valid, then $\boldsymbol{f}_{ij}^{fric} = \boldsymbol{f}_{ij}^{fric,\mathrm{trial}}$, $\Delta\boldsymbol{x}_{ij} = \Delta\boldsymbol{x}_{ij}^{\mathrm{trial}}$ and $\boldsymbol{t}_{ij} = \boldsymbol{t}_{ij}^{\mathrm{trial}}$; otherwise, $\boldsymbol{f}_{ij}^{fric} = \mu_D \left\| \boldsymbol{f}_{ij}^{con} \right\| \boldsymbol{t}_{ij}$, wherein μ_D is the dynamic friction coefficient and $\boldsymbol{t}_{ij} = \boldsymbol{t}_{ij}^{\mathrm{trial}}$ is the sliding direction, which is equal to the direction of the trial friction force. In the latter case, the elongation of the spring is not the trial elongation. However, it may be obtained from the trial elongation by means of a correction term $\Delta\boldsymbol{x}_{ij}^{\mathrm{corr}}$, such that the maximum elongation possible (which is the elongation corresponding to the static friction limit) is not exceeded:

$$\Delta\boldsymbol{x}_{ij} = \Delta\boldsymbol{x}_{ij}^{\mathrm{trial}} - \Delta\boldsymbol{x}_{ij}^{\mathrm{corr}} = \left(\frac{\left\| \boldsymbol{f}_{ij}^{fric,\mathrm{trial}} \right\|}{k^{fric}} - \frac{\left\| \boldsymbol{f}_{ij}^{fric,\mathrm{trial}} \right\| - \mu_S \left\| \boldsymbol{f}_{ij}^{con} \right\|}{k^{fric}} \right) \boldsymbol{t}_{ij}^{\mathrm{trial}} = \frac{\mu_S \left\| \boldsymbol{f}_{ij}^{con} \right\|}{k_{ij}^{fric}} \boldsymbol{t}_{ij}^{\mathrm{trial}}. \tag{33}$$

This is analogous to the return mapping schemes of plasticity models. At the end, the elongation experienced by the spring must be stored as follows

$$\Delta\boldsymbol{x}_{ij}^{\mathrm{accum}} \leftarrow \Delta\boldsymbol{x}_{ij}\,, \tag{34}$$

such that it may be available for computations of subsequent configurations of the system. Additionally, in order to account for the rotation of the tangent contact plane between two successive configurations, the accumulated elongation must be projected onto the current tangent plane as below

$$\Delta\boldsymbol{x}_{ij}^{\mathrm{accum}} \leftarrow \Delta\boldsymbol{x}_{ij}^{\mathrm{accum}} - (\Delta\boldsymbol{x}_{ij}^{\mathrm{accum}} \cdot \boldsymbol{n}_{ij})\boldsymbol{n}_{ij}\,. \tag{35}$$

The only missing quantity in this model is the trial incremental elongation $\delta\boldsymbol{x}_{ij}^{\mathrm{trial}}$ of equation (26). This is given here by

$$\delta\boldsymbol{x}_{ij}^{\mathrm{trial}} = \int_{t_{pr}}^{t} \boldsymbol{v}_{rel,t}^{\mathrm{p}}(\tau) d\tau\,, \tag{36}$$

where t_{pr} is the time instant of the previous configuration at which the accumulated elongation $\Delta\boldsymbol{x}_{ij}^{\mathrm{accum}}$ is known, and t is the time at the current configuration. The integration above is computed here as follows

$$\delta\boldsymbol{x}_{ij}^{\mathrm{trial}} \cong \Big[(1-\varphi)\boldsymbol{v}_{rel,t}^{\mathrm{p}}(t_{pr}) + \varphi\boldsymbol{v}_{rel,t}^{\mathrm{p}}(t) \Big] (t - t_{pr}), \quad 0 \leq \varphi \leq 1. \tag{37}$$

The stiffness of the tangential spring is taken here following Mindlin´s solution for elastic tangential deformation of contacting spheres, such that

$$k^{fric} = 8G^* \sqrt{r^*} \left| \delta_{ij} \right|^{1/2}, \quad \text{with} \quad G^* = \frac{G_i G_j}{G_i + G_j} \tag{38}$$

(G^* is the effective shear modulus of the contacting pair), whereas the damping constant of the dashpot is

$$d^{fric} = 2\xi_t \sqrt{m^* k^{fric}}\,, \tag{39}$$

with ξ_t as the tangential damping rate. More details can be found in Campello (2016).

3.8 Friction moment

The moment generated by the friction forces on particle i (relatively to the center of the particle) is given by

$$\boldsymbol{m}_i^{fric} = \sum_{j=1}^{N_i^{con}} \boldsymbol{r}_i^{\mathrm{P}} \times \boldsymbol{f}_{ij}^{fric}, \tag{40}$$

where we recall that $\boldsymbol{r}_i^{\mathrm{P}}$ is the vector that connects the center of the particle to the contacting point P with particle j (see Fig. 2, bottom part).

Remark. The effect of Magnus forces on the motion of the particles are assumed to be negligible in this work, although they could have been easily incorporated. In such case, one extra term $\boldsymbol{f}_i^{mag} = S\boldsymbol{\omega}_i \times \boldsymbol{v}_i$ ($S =$ given constant) would have to be added to equation (3). Magnus forces arise whenever a particle has non-zero spin and non-zero translational velocity, as an effect of unequal drag forces experienced by the particle throughout its surface (the relative velocity between the particle surface and the surrounding fluid varies for each point of the particle´s surface, due to the contribution of the particle's spin).

3 TIME INTEGRATION SCHEME

Our scheme for solution of the system´s dynamics starts by performing time integration of equation (2) between time instants t and $t + \Delta t$, which furnishes

$$\begin{aligned} \boldsymbol{v}_i(t+\Delta t) &= \boldsymbol{v}_i(t) + \frac{1}{m_i}\int_t^{t+\Delta t} \boldsymbol{f}_i^{tot} dt\,, \\ \boldsymbol{\omega}_i(t+\Delta t) &= \boldsymbol{\omega}_i(t) + \frac{1}{j_i}\int_t^{t+\Delta t} \boldsymbol{m}_i^{tot} dt\,. \end{aligned} \tag{41}$$

The integrals on the right-hand side of (41) are then approximated by using a generalized trapezoidal rule:

$$\begin{aligned} \int_t^{t+\Delta t} \boldsymbol{f}_i^{tot} dt &\approx \Big[\phi \boldsymbol{f}_i^{tot}(t+\Delta t) + (1-\phi)\boldsymbol{f}_i^{tot}(t)\Big]\Delta t\,, \\ \int_t^{t+\Delta t} \boldsymbol{m}_i^{tot} dt &\approx \Big[\phi \boldsymbol{m}_i^{tot}(t+\Delta t) + (1-\phi)\boldsymbol{m}_i^{tot}(t)\Big]\Delta t\,, \end{aligned} \tag{42}$$

in which $0 \leq \phi \leq 1$. When $\phi = 0$, the integration amounts to an (explicit) forward Euler scheme; when $\phi = 1$, to an (implicit) backward Euler one; and when $\phi = 0.5$, to an (implicit) classical trapezoidal rule. By inserting (42) into (41), we have

$$\begin{aligned} \boldsymbol{v}_i(t+\Delta t) &= \boldsymbol{v}_i(t) + \frac{\Delta t}{m_i}\Big[\phi \boldsymbol{f}_i^{tot}(t+\Delta t) + (1-\phi)\boldsymbol{f}_i^{tot}(t)\Big], \\ \boldsymbol{\omega}_i(t+\Delta t) &= \boldsymbol{\omega}_i(t) + \frac{\Delta t}{j_i}\Big[\phi \boldsymbol{m}_i^{tot}(t+\Delta t) + (1-\phi)\boldsymbol{m}_i^{tot}(t)\Big]. \end{aligned} \tag{43}$$

On the other hand, by time integration of the velocity and incremental rotation vectors between t and $t + \Delta t$ we have

$$\begin{aligned} \boldsymbol{x}_i(t+\Delta t) &= \boldsymbol{x}_i(t) + \int_t^{t+\Delta t} \boldsymbol{v}_i dt \,, \\ \boldsymbol{\alpha}_i^{\Delta}(t+\Delta t) &= \int_t^{t+\Delta t} \boldsymbol{\omega}_i dt \,. \end{aligned} \tag{44}$$

The generalized trapezoidal rule is then invoked again to approximate the integrals on the right-hand side of (44), rendering

$$\begin{aligned} \int_t^{t+\Delta t} \boldsymbol{v}_i dt &\approx \big[\phi \boldsymbol{v}_i(t+\Delta t) + (1-\phi)\boldsymbol{v}_i(t)\big]\Delta t \,, \\ \int_t^{t+\Delta t} \boldsymbol{\omega}_i dt &\approx \big[\phi \boldsymbol{\omega}_i(t+\Delta t) + (1-\phi)\boldsymbol{\omega}_i(t)\big]\Delta t \,. \end{aligned} \tag{45}$$

By introducing (45) into (44), we arrive at

$$\begin{aligned} \boldsymbol{x}_i(t+\Delta t) &= \boldsymbol{x}_i(t) + \big[\phi \boldsymbol{v}_i(t+\Delta t) + (1-\phi)\boldsymbol{v}_i(t)\big]\Delta t \,, \\ \boldsymbol{\alpha}_i^{\Delta}(t+\Delta t) &= \big[\phi \boldsymbol{\omega}_i(t+\Delta t) + (1-\phi)\boldsymbol{\omega}_i(t)\big]\Delta t \,. \end{aligned} \tag{46}$$

Expressions (43) and (46) constitute a set of equations for $i = 1,...,N_P$ particles, with which the velocity, spin, position and incremental rotation vectors of each particle at $t+\Delta t$ may be computed once $\boldsymbol{v}_i(t)$, $\boldsymbol{\omega}_i(t)$ and $\boldsymbol{x}_i(t)$ are known. This computation, however, cannot be performed directly, since (43) requires the evaluation of $\boldsymbol{f}_i^{tot}(t+\Delta t)$ and $\boldsymbol{m}_i^{tot}(t+\Delta t)$, which in turn are functions of all unknown position, velocity, spin and incremental rotation vectors at $t+\Delta t$, i.e.,

$$\begin{aligned} \boldsymbol{f}_i^{tot}(t+\Delta t) &= \hat{\boldsymbol{f}}_i^{tot}\ \ \boldsymbol{x}_j(t+\Delta t), \boldsymbol{v}_j(t+\Delta t), \boldsymbol{\omega}_j(t+\Delta t), \boldsymbol{\alpha}_j^{\Delta}(t+\Delta t)\ \ , \\ \boldsymbol{m}_i^{tot}(t+\Delta t) &= \hat{\boldsymbol{m}}_i^{tot}\ \ \boldsymbol{x}_j(t+\Delta t), \boldsymbol{v}_j(t+\Delta t), \boldsymbol{\omega}_j(t+\Delta t), \boldsymbol{\alpha}_j^{\Delta}(t+\Delta t)\ \ , \end{aligned} \tag{47}$$

wherein $j = 1,2,...,N_P$ (the notation with a superposed hat above has been introduced to indicate that the quantity is a function of the arguments inside the parentheses). This means that all equations are strongly coupled and a recursive solution strategy is thereby necessary. We adopt here a fixed-point iterative scheme, following the ideas that have been proposed by Campello and Zohdi (2014a, 2014b) for irrotational particles (i.e. particles without rotational DOFs). The main steps are as summarized in Algorithm 1 below. The scheme is relatively easy to be implemented and it is noteworthy that no system matrix is required.

Finally, after convergence, the total rotation vector of the particles is updated by means of the Rodrigues expression (see Campello (2015) and Campello (2016)):

$$\boldsymbol{\alpha}_i(t+\Delta t) = \frac{4}{4 - \boldsymbol{\alpha}_i(t)\cdot\boldsymbol{\alpha}_i^{\Delta}(t+\Delta t)}\left(\boldsymbol{\alpha}_i(t) + \boldsymbol{\alpha}_i^{\Delta}(t+\Delta t) - \frac{1}{2}\boldsymbol{\alpha}_i(t)\times\boldsymbol{\alpha}_i^{\Delta}(t+\Delta t)\right). \tag{48}$$

Remark. According to what is described in Algorithm 1, one may find that velocities, spins, positions and incremental rotations of all particles are updated only after one complete loop of step (3). This would correspond to a Jacobi-type of scheme and is presented like so only for the sake of algebraic simplicity. What we actually do in step (3) is: for each particle i, we compute $\boldsymbol{f}_i^{tot,K+1}(t+\Delta t)$ and $\boldsymbol{m}_i^{tot,K+1}(t+\Delta t)$ using the velocities, spins, positions and incremental rotations of the particles that have just been updated within the current loop, that is, using $\boldsymbol{v}_j^{K+1}(t+\Delta t)$, $\boldsymbol{\omega}_j^{K+1}(t+\Delta t)$, $\boldsymbol{x}_j^{K+1}(t+\Delta t)$ and $\boldsymbol{\alpha}_j^{\Delta,K+1}(t+\Delta t)$, $j = 1,2,...,i-1$. For $j \geq i$, the values of the previous iteration, i.e., $\boldsymbol{v}_j^{K}(t+\Delta t)$, $\boldsymbol{\omega}_j^{K}(t+\Delta t)$, $\boldsymbol{x}_j^{K}(t+\Delta t)$ and $\boldsymbol{\alpha}_j^{\Delta,K}(t+\Delta t)$, are used. This resembles a Gauss-Seidel scheme, which, as it is well known,

Algorithm 1. Time integration scheme for solution of the system´s dynamics

1. Known (given) quantities:
   $t = 0$, $\Delta t =$ known, $\phi =$ known, $\boldsymbol{x}_i(t)$, $\boldsymbol{\alpha}_i(t)$, $\boldsymbol{v}_i(t)$, $\boldsymbol{\omega}_i(t) =$ known
2. Initialize time step:
   $K = 0$ (iteration counter)
   $\boldsymbol{x}_i^K(t+\Delta t) = \boldsymbol{x}_i(t)$, $\boldsymbol{\alpha}_j^{\Delta,K}(t+\Delta t) = \boldsymbol{o}$,
   $\boldsymbol{v}_i^K(t+\Delta t) = \boldsymbol{v}_i(t)$, $\boldsymbol{\omega}_i^K(t+\Delta t) = \boldsymbol{\omega}_i(t)$ (predictor)
3. Loop over particles: FOR $i = 1,\ldots,N_P$ DO
   i. Compute force and moment vectors at $t+\Delta t$:
   $\boldsymbol{f}_i^{tot,K+1}(t+\Delta t) = \hat{\boldsymbol{f}}_i^{tot} \quad \boldsymbol{x}_j^K(t+\Delta t), \boldsymbol{v}_j^K(t+\Delta t), \boldsymbol{\omega}_j^K(t+\Delta t), \boldsymbol{\alpha}_j^{\Delta,K}(t+\Delta t)$
   $\boldsymbol{m}_i^{tot,K+1}(t+\Delta t) = \hat{\boldsymbol{m}}_i^{tot} \quad \boldsymbol{x}_j^K(t+\Delta t), \boldsymbol{v}_j^K(t+\Delta t), \boldsymbol{\omega}_j^K(t+\Delta t), \boldsymbol{\alpha}_j^{\Delta,K}(t+\Delta t)$
   ii. Update velocity and spin vectors:
   $$\boldsymbol{v}_i^{K+1}(t+\Delta t) = \boldsymbol{v}_i(t) + \frac{\Delta t}{m_i}\Big[\phi \boldsymbol{f}_i^{tot,K+1}(t+\Delta t) + (1-\phi)\boldsymbol{f}_i^{tot}(t)\Big]$$
   $$\boldsymbol{\omega}_i^{K+1}(t+\Delta t) = \boldsymbol{\omega}_i(t) + \frac{\Delta t}{j_i}\Big[\phi \boldsymbol{m}_i^{tot,K+1}(t+\Delta t) + (1-\phi)\boldsymbol{m}_i^{tot}(t)\Big]$$
   iii. Update position and incremental rotation vectors
   $$\boldsymbol{x}_i^{K+1}(t+\Delta t) = \boldsymbol{x}_i(t) + \Big[\phi \boldsymbol{v}_i^{K+1}(t+\Delta t) + (1-\phi)\boldsymbol{v}_i(t)\Big]\Delta t$$
   $$\boldsymbol{\alpha}_i^{\Delta,K+1}(t+\Delta t) = \Big[\phi \boldsymbol{\omega}_i^{K+1}(t+\Delta t) + (1-\phi)\boldsymbol{\omega}_i(t)\Big]\Delta t$$
4. Check for convergence
   i. Compute errors $err(\boldsymbol{v})$, $err(\boldsymbol{\omega})$, $err(\boldsymbol{x})$ and $err(\boldsymbol{\alpha}^{\Delta})$
   ii. IF $ANY(error) > TOL \Rightarrow K = K+1$, $GOTO$ (3) (iterate)
   iii. IF $ALL(errors) \leq TOL \Rightarrow t = t + \Delta t$, update $\boldsymbol{\alpha}_i$ and $GOTO$ (2) (next time step)

converges at a faster rate than the Jacobi method (if the Jacobi method converges) or diverges at a faster rate (if the Jacobi method diverges).

Remark. The error measures in step (4) of the algorithm are taken as normalized (nondimensional) measures, and are given by

$$err(\boldsymbol{a}) = \frac{\sum_{i=1}^{N_p}\left\|\boldsymbol{a}_i^{K+1}(t+\Delta t) - \boldsymbol{a}_i^{K}(t+\Delta t)\right\|}{\sum_{i=1}^{N_p}\left\|\boldsymbol{a}_i^{K+1}(t+\Delta t) - \boldsymbol{a}_i(t)\right\|}, \quad \boldsymbol{a} = \boldsymbol{x}, \boldsymbol{v}, \boldsymbol{\omega} \text{ and } \boldsymbol{\alpha}^{\Delta}\ . \tag{49}$$

In cases where the denominator in (49) vanishes or approaches zero, we use

$$err(\boldsymbol{a}) = \frac{\sum_{i=1}^{N_p}\left\|\boldsymbol{a}_i^{K+1}(t+\Delta t) - \boldsymbol{a}_i^{K}(t+\Delta t)\right\|}{\sum_{i=1}^{N_p}\left\|\boldsymbol{a}_i^{K+1}(t+\Delta t)\right\|}, \quad \boldsymbol{a} = \boldsymbol{x}, \boldsymbol{v}, \boldsymbol{\omega} \text{ and/or } \boldsymbol{\alpha}^{\Delta}, \tag{50}$$

instead.

4 NUMERICAL EXAMPLES

In this section, we provide a few examples of numerical simulations to illustrate how our

DEM formulation may be used to study granular materials. We adopt $\phi = 0.5$ in the time integration scheme throughout, meaning that an implicit classical trapezoidal rule is utilized in all cases. Selection of the time step size is made according to the duration of a typical contact/collision for the problem at hand. We use the following criterion:

$$\Delta t_{con} \cong 2.87\left[\frac{(m^*)^2}{r^*(E^*)^2 v_{rel}}\right]^{1/5} \Rightarrow \ \Delta t \leq \frac{\Delta t_{con}}{20}\,, \tag{51}$$

where Δt_{con} is the duration of a typical contact or collision and v_{rel} is the relative velocity of a typical contacting pair in the pair´s central direction immediately before the contact/collision is initiated. This is based on Hertz´s formula for the duration of elastic collisions and, according to our experience, allows for a good accuracy in the integration of the contact forces. The convergence tolerance used within the iterations (step 4 of Algorithm 1) is $TOL = 10^{-6}$.

4.1 Particle size segregation in a vertically vibrated container

This example is proposed by Pöschel and Schwager (2004) and is reproduced here with some slight modifications. A granular material comprised of $N_P = 1000$ spherical particles is deposited by gravity in a container wherein a large particle rests at the bottom, as shown in Fig. 3, top left. The dimensions of the container are 0.4 m (base) and 1.0 m (height), whereas the radii of the particles follow a Gaussian distribution of mean value $\overline{r} = 0.01$ m and standard deviation $\sigma_r = 0.001$ m (the distribution is truncated at two standard deviations from the mean, such that all radii lie in the interval [0.008 m, 0.012 m]). The larger particle has $r = 0.06$ m. As in Pöschel and Schwager (2004), the walls of the container are modeled by particles whose relative positions (w.r.t. each other) are held fixed, as in the case of a prescribed "boundary condition". This allows for the representation (though in a very simplified way) of the roughness of the container. Once the material is at rest, the container is set to vibrate vertically according to $y(t) = A\,\mathrm{sen}(\omega t)$, with amplitude $A = 0.02$ m and angular frequency $\omega = 30$ rad/s. Other data are as follows:

- wall particles radii: $r_W = 0.01$ m;
- mass-density of the particles: $\rho = 8000$ kg/m^3;
- elastic properties of the particles: $E = 10^9$ N/m^2 and $\nu = 0$;
- friction coefficients (between all particles, including wall particles): $\mu_S = \mu_D = 0.5$;
- damping rates: $\xi_n = 0.0002$ and $\xi_t = 0.02$;
- gravity acceleration: $g = -9.81$ m/s^2 (y-direction);
- time-step size: $\Delta t = 2.5\times 10^{-5}$ s (with time adaptivity, wherein $\Delta t_{\max} = \Delta t$ and $\Delta t_{\min} = 0.1\Delta t$).

Drag, near-field and adhesion forces are not considered. We remark that the damping parameters here are different from those of Pöschel and Schwager (2004), for in this reference different contact and friction models are adopted. Figure 3 shows snapshots of the system´s configuration at selected time instants, as obtained with our simulation. One can see how the larger particle advances toward the top of the container and, at around $t \approx 20$ s, emerges at the "surface" of the material. Figure 3, bottom part, depicts the time evolution of the vertical coordinate of the particle, wherein it can be observed that the ascending motion is cyclic (as

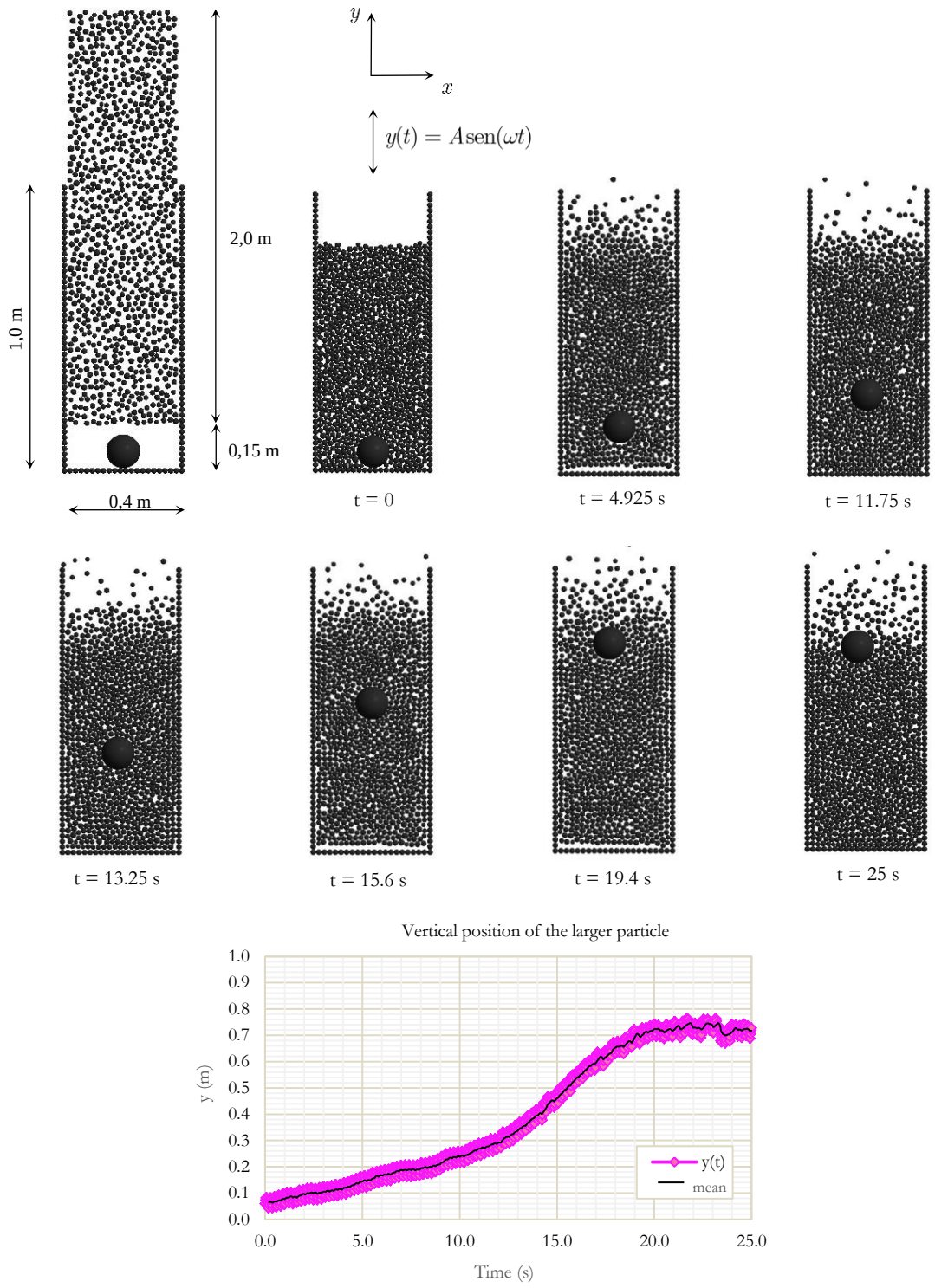

Fig. 3 Particle size segregation in a vertically vibrated container. Problem definition and analysis results

expected) and occurs with varying velocity over time (this can be explained by the variation in the material´s bulk density along the container´s height). This example illustrates a phenomenon that is typical of granular materials: the size segregation of grains by shaking or vibration. In the physics of granular materials, this is known as the *Brazil nuts effect*. It is instructive to observe that, if this problem is analyzed with no rotational degress-of-freedom, size segregation does not show up (see Campello (2016)).

4.2 Dismantling of a pile of grains

A certain amount of granular material is piled vertically (with lateral constraints) over a flat rigid surface, forming a prism of squared base as shown in Fig. 4, top part (the lateral constraints are not shown for simplicity). Gravity acts in the vertical (-y) direction. With the grains at rest, the constraints are removed abruptly and the pile experiences a small avalanche, dismantling into a mound of grains shortly thereafter. The size and shape of this mound depends fundamentally on the friction of the grains, and this aspect is briefly investigated here. The pile has initial dimensions of 1.0 m (sides) and 0.7 m (height). The grains, in turn, are spherical and have their radii following a Gaussian distribution of mean $\overline{r} = 0.02$ m and standard deviation $\sigma_r = 0.002$ m (the distribution is truncated at three standard deviations from the mean, such that all radii lie in the interval [0.014 m, 0.026 m]). The volume fraction of the pile (ratio of total volume of the particles to the volume of the prism) is 0.57. Five different simulations are conducted, each one corresponding to a different set of friction parameters for the grains:

- simulation 1: $\mu_S = \mu_D = 0$ and $\mu_R = 0$;
- simulation 2: $\mu_S = \mu_D = 0.15$ and $\mu_R = 0.05$;
- simulation 3: $\mu_S = \mu_D = 0.25$ and $\mu_R = 0.1$;
- simulation 4: $\mu_S = \mu_D = 0.5$ and $\mu_R = 0.45$;
- simulation 5: $\mu_S = \mu_D = 1$ and $\mu_R = 0.9$.

In the above, μ_R stands for the rolling resistance coefficient (see Campello (2016) for details). Other data are as follows:

- mass-density of the particles: $\rho = 2500$ kg/m^3;
- elastic properties of the particles: $E = 2 \times 10^7$ N/m^2 and $\nu = 0.25$;
- friction parameters of the particles with the rigid surface: $\mu_S = \mu_D = 0.65$, with μ_R taken as the same as the particle-particle corresponding case;
- damping rates: $\xi_n = \xi_t = 0.1$;
- gravity acceleration: $g = -9,81$ m/s^2 (y-direction);
- time-step size: $\Delta t = 1 \times 10^{-4}$ s (with time adaptivity, wherein $\Delta t_{\max} = \Delta t$ and $\Delta t_{\min} = 0.1 \Delta t$);
- total number of particles in the pile: $N_P = 12360$.

These values are taken from Yan et al. (2015), who also studied piles of grains (though from a different perspective and problem setting). Drag, near-field and adhesion forces are not considered. Figure 4 depicts snapshots of the system´s configuration at selected time instants as obtained in a typical simulation (the case shown is for simulation 5; results for the other simulations are not shown for brevity). As it can be seen, after collapsing and attaining static equilibrium, the pile turns into a mound with the shape of a shallow cone, as expected. The aspect ratio of such cone can be characterized by the angle of repose θ, which is computed here as the average of the slopes of the mound, as obtained in two orthogonal cross-sections aligned with the reference axes. Table 1 shows the values of θ obtained in each one of the five simulations, and Fig. 4, bottom part, shows the final configuration for each case (side view).

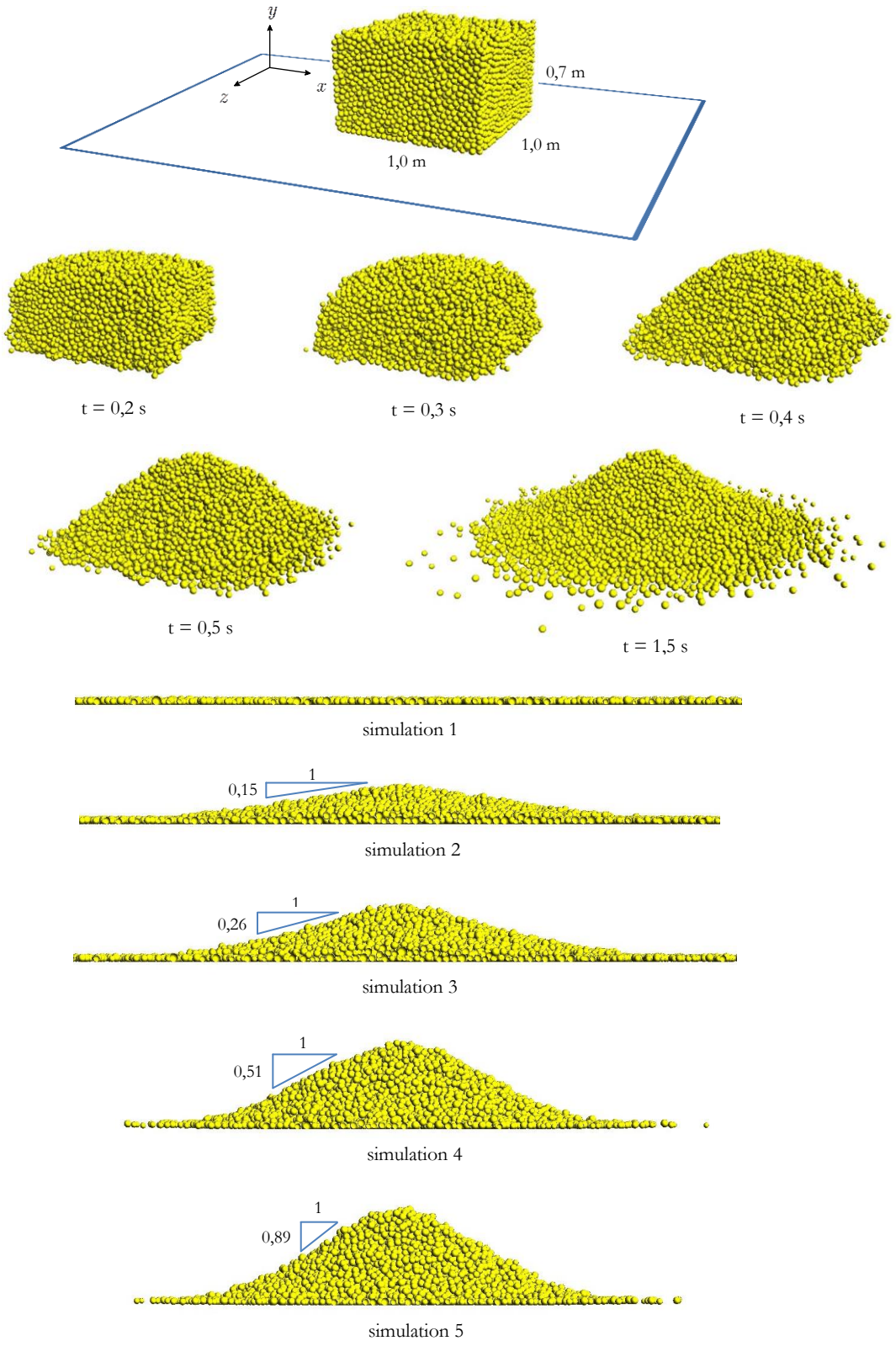

Fig. 4 Dismantling of a pile of grains. Problem definition and analysis results

Table 1. Dismantling of a pile of grains. Angle of repose.

Friction parameters	Average slope ($\tan\theta$)	Angle of repose (θ)
Simulation 1	0	0
Simulation 2	0.15	8.5º
Simulation 3	0.26	14.5 º
Simulation 4	0.51	27.0º
Simulation 5	0.89	41.7º

4.3 Deposition of particles onto a rigid surface

A jet of particles is projected onto a rigid surface with the aim that they adhere and provide a protective layer to the surface, as indicated in Fig. 5, top part. We want to investigate what is the appropriate projection velocity v_x such that good adherence and good visual aspect are observed for the deposited layer. The jet consists of $N_P = 1500$ spherical particles (placed randomly within a fictitious prism of dimensions 15 cm x 2.5 cm x 2.5 cm), the radii of which follow a Gaussian distribution of mean $\bar{r} = 2.0$ mm and standard deviation $\sigma_r = 0.2$ mm (the distribution is truncated at three standard deviations from the mean such that all radii lie in the interval [1.4 mm, 2.6 mm]). The jet moves in the positive y-direction at a constant speed of 5 m/s. The adhesion of the particles with the surface (and also with themselves) is represented by forces in the form of equations (16)-(17). Drag forces given by equation (6) are also considered (the medium surrounding the particles is the air). Other parameters are:

- mass-density of the particles: $\rho = 1000$ kg/m^3;
- elastic properties of the particles: $E = 1\times10^7$ N/m^2 and $\nu = 0.25$;
- friction coefficient between particles: $\mu_S = \mu_D = 0.05$;
- friction coefficient between particles and the rigid surface: $\mu_S = \mu_D = 0.4$;
- rolling resistance coefficient between particles: $\mu_R = 0.1$;
- rolling resistance coefficient between particles and the rigid surface: $\mu_R = 0.25$;
- damping rates (particle-particle and particle-rigid surface): $\xi_n = 0.8$ and $\xi_t = 0.1$;
- adhesion force parameters: $k^{adh} = 10^3$ N/m and $\beta = 3/2$;
- fluid mass-density and viscosity (air): $\rho_F = 1.2$ kg/m^3 and $\eta_F = 1.8\times10^{-5}$ Pa·s;
- jet projection velocity: $v_x = 1,\ 5,\ 10$ and 20 m/s;
- gravity acceleration: $g = -9.81$ m/s^2 (y-direction);
- time-step size: $\Delta t = 1\times10^{-4}$ s;
- time at the end of the simulation: $t_F = 1.0$ s.

Figure 10 shows snapshots of the simulation at selected time instants for each one of the projection velocities considered. As it can be observed, the case with $v_x = 1$ m/s is not able to enforce adherence. For the other cases, however, there is practically complete adherence plus good coherence, though the visual aspect of the layer is quite different for each velocity. When $v_x = 5$ m/s, the layer is long, narrow and thin; when $v_x = 10$ m/s, it is less long and a bit wider and thicker than the previous case; and when $v_x = 20$ m/s, it has a very compact aspect, being also thicker. Each one of these characteristics may be more or less desirable, depending on the application one is interested in. Table 2 provides values of the mean thickness and length of the layer for each case.

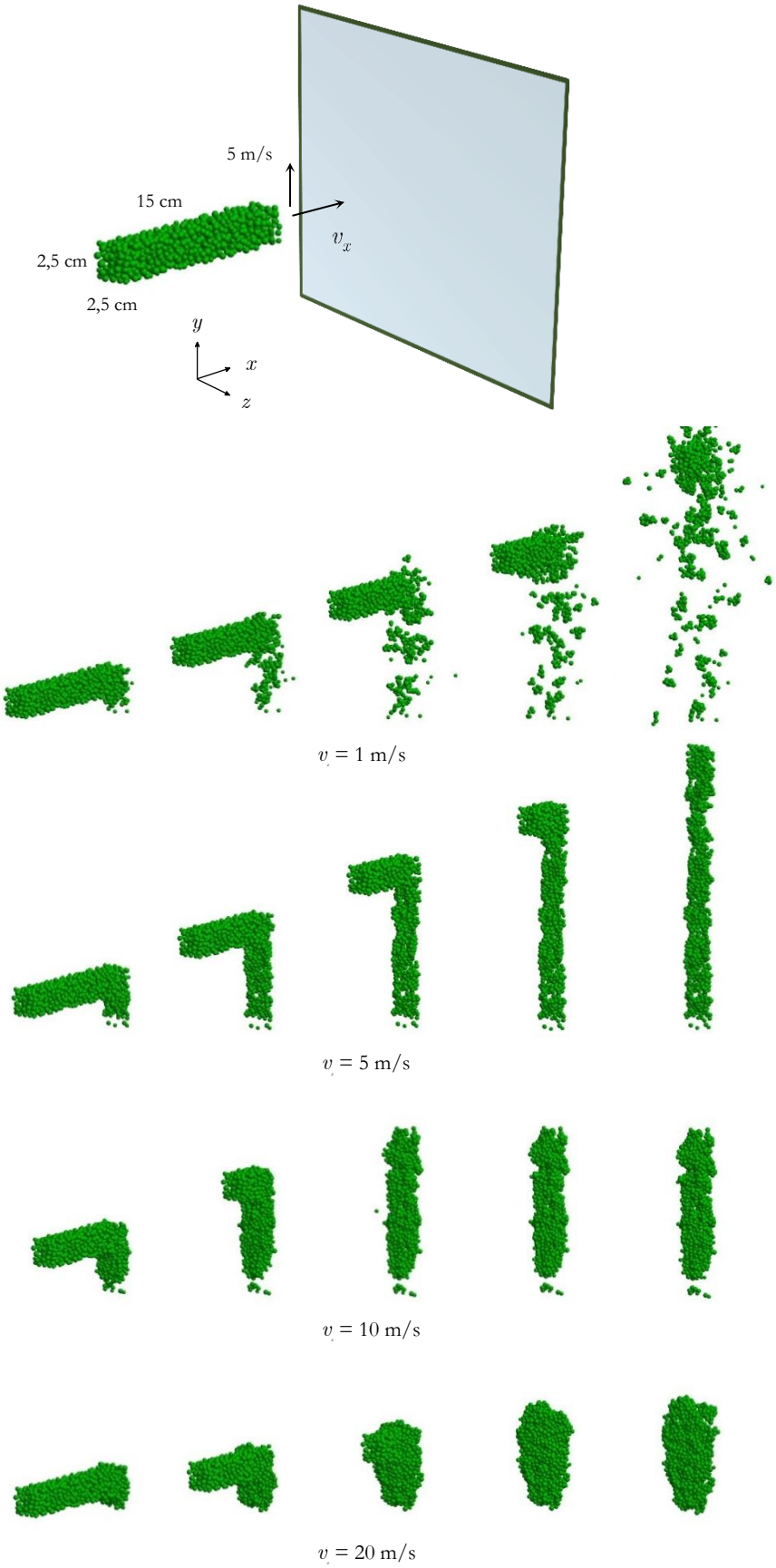

Fig. 5 Deposition of particles onto a rigid surface. Problem definition and analysis results

Table 2. Deposition of particles onto a rigid surface. Layer properties.

Projection velocity	Layer mean thickness (standard deviation in parentheses)	Layer length
1 m/s	--	--
5 m/s	0,9 cm (0,42 cm)	34 cm
10 m/s	1,4 cm (0,61 cm)	18 cm
20 m/s	1,6 cm (0,72 cm)	13 cm

5 CONCLUSIONS

The main purpose of this work was to present a simple computational model for the simulation of real problems involving granular materials. Many natural phenomena and industrial applications may be studied with models of such type. A few numerical examples were provided to illustrate the potentialities of the scheme. The interested reader is referred to a recent work by the author in Campello (2016) for more details on the formulation and a more complete set of numerical examples. The author believes that consistent DEM models are a very useful tool for the study of granular materials and, in a broader sense, of particle systems.

ACKNOWLEDGEMENTS

This work was supported by CNPq (Conselho Nacional de Desenvolvimento Científico e Tecnológico) and FAPESP (São Paulo State Science Foundation), under the grants 303793/2012-0 and 2014/19821-7, respectively. Support from CMRL (Computational Materials Research Laboratory, University of California at Berkeley, USA), and from colleague Tarek Zohdi, is likewise gratefully acknowledged.

REFERENCES

Bicanic, N., 2004. Discrete Element Methods. In: Stein E, de Borst R, Hughes TJR (eds) *Encyclopedia of Computational Mechanics, Volume 1: Fundamentals*. Chichester: John Wiley & Sons.

Biringen, S., Chow, C.-Y., 2011. *An introduction to computational fluid mechanics by example*. Hoboken: Wiley.

Campello, E. M. B., 2016. *Um modelo computacional para o estudo de materiais granulares*. Tese de Livre-Docência, Escola Politécnica da Universidade de São Paulo. 100p.

Campello, E. M. B., 2015a. A description of rotations for DEM models of particle systems. *Computational Particle Mechanics* 2:109–125.

Campello, E. M. B., 2015b. Computational modeling and simulation of rupture of membranes and thin films. *Journal of the Brazilian Society of Mechanical Sciences and Engineering* 37:1793-1809.

Campello, E. M. B., Cassares, K. R., 2016. Rapid generation of particle packs at high packing ratios for DEM simulations of granular compacts. *Latin American Journal of Solids and*

Structures 13:23-50.

Campello, E. M. B., Zohdi, T., 2014a. A computational framework for simulation of the delivery of substances into cells. *International Journal for Numerical Methods in Biomedical Engineering* 30:1132–1152.

Campello, E. M. B., Zohdi, T., 2014b. Design evaluation of a particle bombardment system used to deliver substances into cells. *Computer Modeling in Engineering & Sciences* 98(2):221–245.

Duran, J., 1997. *Sands, Powders and Grains: An introduction to the physics of granular matter*. New York: Springer.

Johnson, K. L., 1985. *Contact Mechanics*. Cambridge: Cambridge University Press.

Lennard-Jones, J. E., 1924. On the Determination of Molecular Fields. Proceedings of the Royal Society of London A 106(738): 463–477.

O´Sullivan, C., 2011. Particle-based discrete element modeling: a Geomechanics perspective. *International Journal of Geomechanics* 11:449–464.

Pöschel, T., Schwager, T., 2004. *Computational Granular Dynamics*. Berlin: Springer.

Wellmann, C., Wriggers, P., 2012. A two-scale model of granular materials. *Computer Methods in Applied Mechanics and Engineering* 205–208:46–58.

Yan, Z., Wilkinson, S. K., Stitt E. H., Marigo M., 2015. Discrete Element Modelling (DEM) input parameters: understanding their impact on model predictions using statistical analysis. *Computational Particle Mechanics* 2:283–299.

Zhu, H. P., Zhou, Z. Y., Yang, R. Y., Yu, A. B., 2008. Discrete particle simulation of particulate systems: a review of major applications and findings. *Chemical Engineering Science* 63:5728–5770.

Zohdi, T. I., 2102. *Dynamics of charged particulate systems: Modeling, theory and computation*. New York: Springer.